Drosophila Cappuccino alleles provide insight into formin mechanism and role in oogenesis

Haneul Yoo[a,*], Elizabeth A. Roth-Johnson[b,*], Batbileg Bor[b], and Margot E. Quinlan[a,c]
[a]Department of Chemistry and Biochemistry, [b]Molecular Biology Interdepartmental PhD Program, and [c]Molecular Biology Institute, University of California, Los Angeles, Los Angeles, CA 90095

ABSTRACT **During *Drosophila* development, the formin actin nucleator Cappuccino (Capu) helps build a cytoplasmic actin mesh throughout the oocyte. Loss of Capu leads to female sterility, presumably because polarity determinants fail to localize properly in the absence of the mesh. To gain deeper insight into how Capu builds this actin mesh, we systematically characterized seven *capu* alleles, which have missense mutations in Capu's formin homology 2 (FH2) domain. We report that all seven alleles have deleterious effects on fly fertility and the actin mesh in vivo but have strikingly different effects on Capu's biochemical activity in vitro. Using a combination of bulk and single- filament actin-assembly assays, we find that the alleles differentially affect Capu's ability to nucleate and processively elongate actin filaments. We also identify a unique "loop" in the lasso region of Capu's FH2 domain. Removing this loop enhances Capu's nucleation, elongation, and F-actin–bundling activities in vitro. Together our results on the loop and the seven missense mutations provides mechanistic insight into formin function in general and Capu's role in the *Drosophila* oocyte in particular.**

Monitoring Editor
Denise Montell
University of California, Santa Barbara

Received: Nov 24, 2014
Revised: Jan 28, 2015
Accepted: Mar 10, 2015

INTRODUCTION

The anterior–posterior and dorsal–ventral body axes of *Drosophila melanogaster* are established during mid-oogenesis by the localization of several polarity determinants. The maternal-effect gene *cappuccino* (*capu*) is required for proper localization of posterior polarity determinants, including *oskar* mRNA, and loss of functional Cappuccino (Capu) leads to female sterility (Manseau and Schupbach, 1989; Emmons *et al.*, 1995).

Capu belongs to the FMN family of formin actin nucleators. Like other formins, Capu nucleates actin filaments and remains processively attached to the elongating barbed end of the filament (Pruyne, 2002; Quinlan *et al.*, 2005; Bor *et al.*, 2012). In vivo, Capu helps build a cytoplasmic actin mesh throughout the *Drosophila* oocyte, which can be detected as early as stage 5 and persists through mid-oogenesis (Dahlgaard *et al.*, 2007). Disappearance of this actin mesh around stage 10b coincides with dramatic reorganization of the microtubule cytoskeleton and the onset of fast, microtubule-dependent cytoplasmic streaming (Theurkauf, 1994; Dahlgaard *et al.*, 2007). In *capu* loss-of-function mutants, the actin mesh is not detected; this loss of actin mesh corresponds to premature cytoplasmic streaming, disruption of polarity-determinant localization, and female sterility (Manseau and Schupbach, 1989; Theurkauf, 1994). Recent work has shown that Capu's ability to build this mesh requires its own nucleation and/or processive elongation activity, as well as its ability to bind Spire (Spir), another actin-nucleating protein (Quinlan, 2013). Capu also binds microtubules, the sides of actin filaments, and its own N-terminal autoinhibitory domain (Rosales-Nieves *et al.*, 2006; Quinlan *et al.*, 2007; Bor *et al.*, 2012; Roth-Johnson *et al.*, 2014). How these activities contribute to building the actin mesh and regulating the timing of streaming remains unclear.

Several different *capu* alleles have been reported since the gene was first identified (Manseau and Schupbach, 1989; Emmons *et al.*, 1995; Luschnig *et al.*, 2004; Tanaka *et al.*, 2011). Some of these have been sequenced, and all identified ethyl methanesulfonate (EMS)–generated missense mutations occur in Capu's highly conserved formin homology 2 (FH2) domain (Emmons *et al.*, 1995; Tanaka *et al.*, 2011). Although little work has been done to determine the consequences of these mutations in vitro, one previous study

This article was published online ahead of print in MBoC in Press (http://www.molbiolcell.org/cgi/doi/10.1091/mbc.E14-11-1558) on March 18, 2015.

*These authors contributed equally to this work.

Address correspondence to: Margot E. Quinlan (margot@chem.ucla.edu).

Abbreviations used: Capu, Cappuccino; EMS, ethyl methanesulfonate; FH2, formin homology 2; Spir, Spire; TIRF, total internal reflection fluorescence.

showed that two alleles, *capu*^{1} and *capu*^{2F}, have compromised actin-nucleation and microtubule-bundling activities (Rosales-Nieves *et al.*, 2006). Thus further investigation of existing *capu* alleles to better understand formin function and Capu's role in oogenesis is warranted.

In this study, we sequenced a series of *capu* alleles from earlier screens. We then characterized the physiological and biochemical consequences of the missense mutations. We found that all mutations affected fertility and Capu's ability to build the cytoplasmic mesh, yet not all mutations compromised Capu's actin nucleation activity in vitro. We also characterized the in vitro activity of a Capu mutant lacking a 38–amino acid region between the two highly conserved tryptophan residues in Capu's FH2 domain; this region lies near several EMS-generated missense mutations but appears to be unique to Capu. Our systematic in vivo and in vitro analysis of these Capu mutants provides new insight into how the FH2 domain assembles actin and which of its activities are important to oogenesis.

RESULTS

In vivo characterization of *capu* alleles

Female flies with loss-of-function *capu* mutations exhibit severely reduced fertility, loss of the cytoplasmic actin mesh, and premature onset of fast cytoplasmic streaming (Theurkauf, 1994; Dahlgaard *et al.*, 2007; Quinlan, 2013). We systematically characterized each of these phenotypes for seven EMS-generated *capu* alleles. To avoid effects of possible off-site mutations, all mutant flies were crossed to a deficiency line (Df(2L)ed-dp) and characterized as *capu*/Df heterozygotes. Control experiments with homozygous wild-type flies and +/Df flies showed that deletion of one copy of *capu* does not affect fly fertility (Table 1). All *capu* alleles exhibited reduced fertility, although the effect varied from complete sterility to ~25% fertility. We noticed that many of the larvae from the *capu*^{38}/Df flies (9% hatch rate) died within 1 d after hatching. This phenotype was not observed for the other mutants. Our fertility data suggest the following allelic series: *capu*^{1} = *capu*^{HK3} > *capu*^{A354} > *capu*^{HK38} > *capu*^{2F} > *capu*^{L201} > *capu*^{L219}.

We next examined the cytoplasmic actin mesh in midstage oocytes. Although the mesh density has been shown to be reduced in +/Df oocytes as compared with homozygous wild-type oocytes (Dahlgaard *et al.*, 2007), the actin mesh in +/Df oocytes was still denser than the mesh in all of the mutants (Figure 1, A–H). *capu*^{1} and *capu*^{HK3}, which were both completely sterile in our fertility assays, also exhibited the most severe mesh phenotype: the oocytes were devoid of any mesh structure, similar to what has been observed by others (Dahlgaard *et al.*, 2007). Other mutants, such as *capu*^{A354} and *capu*^{L201}, appeared to have small F-actin aggregates or puncta throughout the cytoplasm but were devoid of any cohesive mesh-like structure (Figure 1, D and G). *capu*^{L219}, the weakest allele in our allelic series, had the most cytoplasmic actin in the form of a sparse, mesh-like structure (Figure 1B). In general, the mesh phenotypes correlate with our fertility assays, suggesting that fertility loss is due largely to these mesh phenotypes.

The actin mesh is believed to inhibit fast cytoplasmic streaming. Fast streaming begins concomitantly with the disappearance of the mesh in the stage 10b oocyte, and disrupting the actin mesh, genetically or pharmacologically, leads to premature cytoplasmic streaming (Dahlgaard *et al.*, 2007). Therefore we examined cytoplasmic streaming as a functional readout of mesh integrity. Consistent with the actin mesh being compromised, all mutant alleles exhibited premature cytoplasmic streaming (Figure 1, A′–H′). We used particle image velocimetry to quantify the speed of streaming in these oocytes (Figure 1I; Quinlan, 2013). On average, streaming was substantially faster than wild type in all of the mutants. Similar to Emmons *et al.* (1995), we did not observe a correlation between the speed of premature streaming and the fertility of these mutants, nor did we detect a correlation between mesh density and streaming velocity. For instance, the streaming velocities of *capu*^{1} and *capu*^{HK3}, which showed the most severe actin mesh phenotypes, were comparable to that of *capu*^{L219}, which showed the least severe mesh phenotype. In addition, *capu*^{HK3} and *capu*^{2F} had outliers with streaming velocities similar to wild type, suggesting that these alleles might be slightly less penetrant than the other alleles. This result could explain the 18% of *capu*^{2F} eggs that hatch, but it is surprising for *capu*^{HK3}, which was completely sterile in our fertility assays.

In sum, the in vivo results from the seven *capu* mutants indicate that they all fail to build a competent actin mesh, leading to premature cytoplasmic streaming and compromised fertility. Whereas the apparent amount of cytoplasmic actin present in the oocyte is consistent with our fertility assays, we did not observe any correlation between streaming velocity and fertility.

Genotype	Percentage hatched	Number counted	Lesion[a]	First reported
w^{1118}	90	449	N/A	N/A
w^{1118}/Df(2L)ed-dp	88	280	N/A	N/A
capu^{L219}/Df(2L)ed-dp	25	374	**K586M**	Luschnig *et al.* (2004)
capu^{2F}/Df(2L)ed-dp	18	369	P597L[b]	Emmons *et al.* (1995)
capu^{A354}/Df(2L)ed-dp	2	297	D662N[c]	Tanaka *et al.* (2011)
capu^{HK3}/Df(2L)ed-dp	0	511	I751T	Manseau and Schupbach (1989)
capu^{1}/Df(2L)ed-dp	1	482	L768H	Manseau and Schupbach (1989)
capu^{L201}/Df(2L)ed-dp	19	242	D854N	Luschnig *et al.* (2004)
capu^{38}/Df(2L)ed-dp	9	221	H977Y	Emmons *et al.* (1995)
capu^{L277}/Df(2L)ed-dp	n.d.	n.d.	**W247stop**	Luschnig *et al.* (2004)

Percentage hatched is reported as the average of three independent trials. Number counted is the sum of eggs counted from all three trials. n.d., not determined.
[a]Bold denotes lesions identified in this study.
[b]Reported as P597T in Emmons *et al.* (1995).
[c]Reported as D670N in Tanaka *et al.* (2011).

TABLE 1: Fertility assays and identified *capu* lesions.

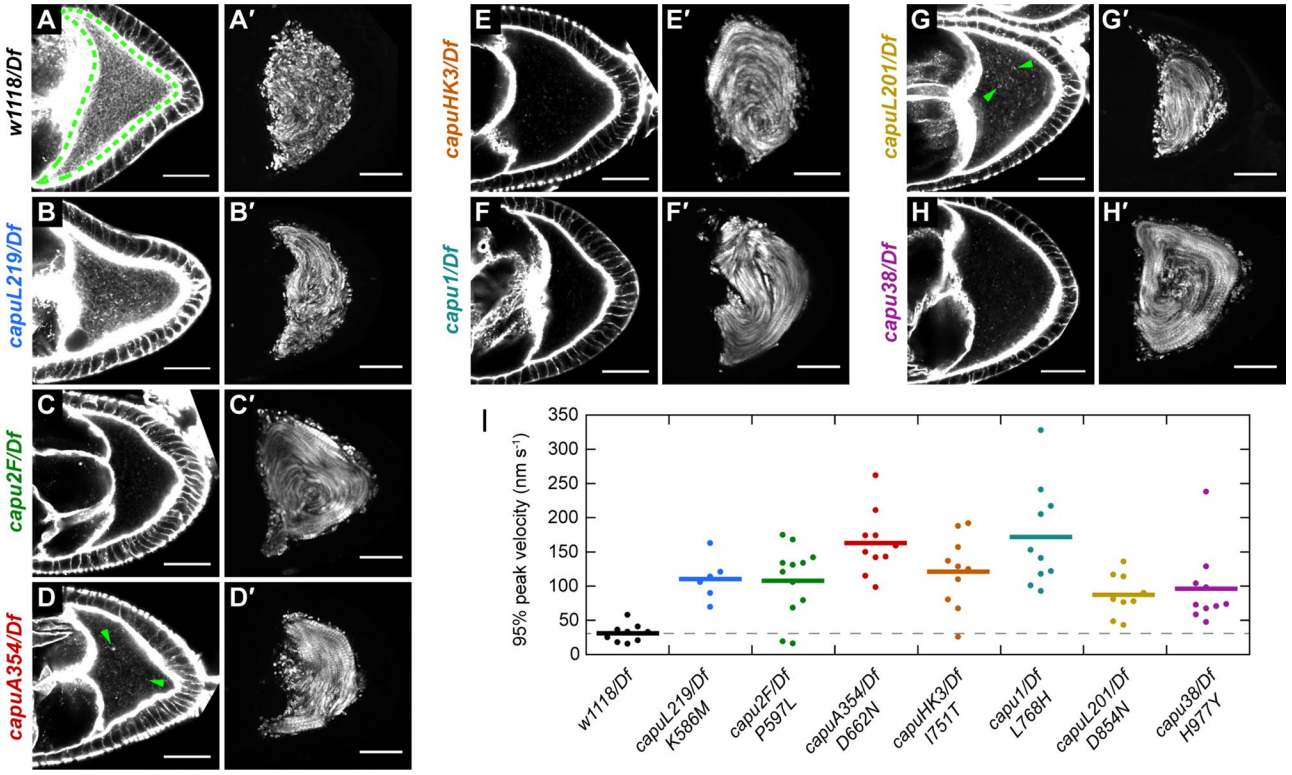

FIGURE 1: EMS-generated *capu* mutants lack actin mesh and exhibit premature streaming. (A–H) Midstage oocytes stained with Alexa Fluor 647–phalloidin to visualize the actin mesh in *capu* mutant flies. The wild-type oocyte is outlined with a green dashed line. A few examples of actin chunks or puncta are indicated by green arrowheads in D and G. (A′–H′) Standard deviation projections of autofluorescent yolk granules over 3 min for typical stage 8-9 oocytes. All scale bars are 30 μm. (I) Quantification of streaming velocities for $n \geq 6$ oocytes from each fly line. Dots represent individual oocytes, and bars represent the mean.

Identification and structural analysis of *capu* missense mutations

Before conducting our in vitro studies, we identified and/or confirmed the causative lesions in each *capu* allele (Table 1). We reported the *capu*^{L201} lesion, D854N, in an earlier article (Roth-Johnson *et al.*, 2014), and identified two previously unknown lesions, K586M and W247stop, in *capu*^{L219} and *capu*^{L277}, respectively. We also identified slightly different mutations for *capu*^{2F} and *capu*^{A354} than originally reported in the literature. Emmons *et al.* (1995) reported P597T as the causative lesion in *capu*^{2F}, but our sequencing revealed a P597L mutation. We used the P597L mutation for our in vitro assays to be consistent with our in vivo analysis. Similarly, Tanaka *et al.* (2011), reported D670N as the causative lesion in *capu*^{A354}, but we identified D662N in our fly line. We confirmed that D670N and D662N are indeed the same lesion; the discrepancy arose from the difference in numbering the FH2 domain (T. Tanaka, personal communication). All of the mutations are in the FH2 domain (Figure 2B), highlighting the functional importance of this domain. We mapped the identified missense mutations on a Capu homology model, which was made based on the crystal structure of hDAAM1 (Arnold *et al.*, 2006; Lu *et al.*, 2007). Using the homology model, we found that the mutations reside in three distinct and structurally important regions of the FH2 domain: the lasso, knob, and post (Xu *et al.*, 2004). Two residues, Lys-586 and Asp-854, in the lasso and post regions, respectively, are well conserved across formin families (Supplemental Figure S1). The hydrophobic residues in the knob region, Ile-751 and Leu-768, are also well conserved. Pro-597 in the lasso is conserved only within the FMN family of formins. Asp-662 and His-977 are poorly conserved if at all.

To study the biochemical consequences of these mutations, we purified each in the context of a C-terminal Capu construct (CapuCT; residues 467–1059) as shown in Figure 2A. All mutant constructs were amenable to purification except CapuCT-L768H. We suspect that mutating this hydrophobic residue to a large, basic residue disrupts the structure of CapuCT, based on its predicted location buried within the globular knob region of the FH2 domain. A neighboring knob mutation, CapuCT-I751T, was also difficult to purify. The yield was ~75% lower than with the wild-type construct.

The lasso/post interface, where many of the mutations are located, is important for dimerization of the FH2 domain (Xu *et al.*, 2004). Therefore, using size exclusion chromatography, we tested whether any of these mutations disrupts dimerization. We compared the elution profiles of the mutants to both CapuCT-W600A, a mutant that cannot dimerize (Vizcarra *et al.*, 2011), and wild-type CapuCT (Figure 2C). SDS–PAGE analysis confirmed the purity of the protein samples injected to the column (Supplemental Figure S2). These data confirmed that CapuCT-D662N, -K586M, -D854N, and -P597L exist predominantly in a dimeric state. Two mutant proteins, CapuCT-I751T and CapuCT-H977Y, had distinct elution profiles. Although a similar quantity of protein was run on the column, CapuCT-I751T did not produce any clear elution peaks, further supporting our hypothesis that this buried hydrophobic mutation disrupts the structure of CapuCT. CapuCT-H977Y eluted primarily as a dimer but exhibited a broader shoulder and an unusually high peak in the void volume. When we reran the dimer peak, it reproducibly eluted as a

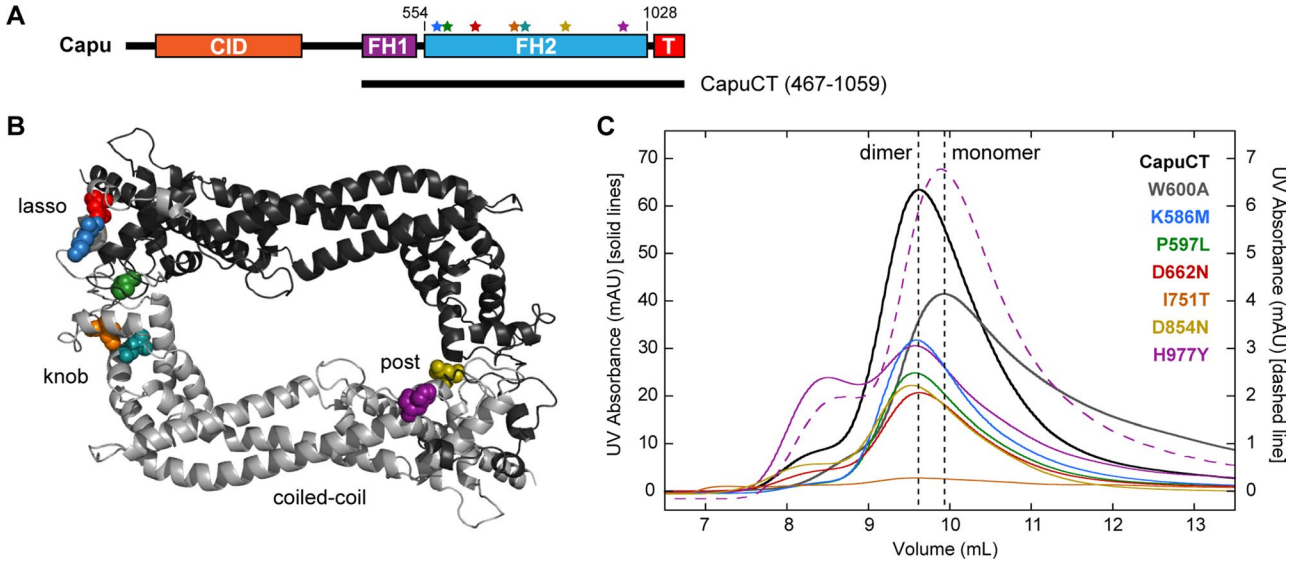

FIGURE 2: Structural analysis of *capu* missense mutations. (A) Domain organization of Capu (1059 amino acids) and schematic of the C-terminal construct used in this study (CapuCT): CID, Capu inhibitory domain; FH1, formin homology 1; FH2, formin homology 2 (residues 554–1028); T, tail. Stars indicate the mutations, which are all located within Capu's FH2 domain. Residues are colored as in other images. (B) Locations of mutated residues within the FH2 domain based on a Capu homology model. The model was generated from the hDAAM1 crystal structure (Protein Data Bank # 2J1D; Lu *et al.*, 2007) using SWISS-MODEL (Arnold *et al.*, 2006). (C) Size exclusion chromatography of all mutants compared with wild-type CapuCT (dimer) and CapuCT-W600A (monomer) controls. The dashed purples line is the elution pattern from running the CapuCT-H977Y dimer peak a second time on the column.

high-volume peak and a new peak, shifted to the right. This elution profile suggests that the CapuCT-H977Y dimer is unstable and/or in equilibrium with a monomer and a higher-order complex/aggregation product.

Effect of *capu* mutations on actin assembly

All of the *capu* alleles that we tested in vivo compromised Capu's ability to build the cytoplasmic actin mesh in the oocyte (Figure 1, A–H). Therefore we hypothesized that all of the mutations would diminish, if not abolish, CapuCT's actin assembly activity. To test our hypothesis, we measured the activity of each mutant in pyrene-actin polymerization assays. All of the mutants showed a dose-dependent increase in actin assembly activity (Supplemental Figure S3). When compared with wild-type CapuCT, many of the mutants exhibited impaired activity in both the presence and absence of excess profilin (Figure 3, A and B). However, this reduction in actin assembly activity varied widely across the different mutants. We used *Schizosaccharomyces pombe* profilin in these assays because, unlike other profilins, it exhibits minimal bias against actin labeled at Cys-374 (unpublished data). The addition of *S. pombe* profilin slowed all of the reactions, but the overall trend in activities remained largely unchanged. We note that only CapuCT-H977Y appeared disproportionately slowed by the presence of profilin compared with the other mutants.

To examine the correlation between the mutants' actin assembly activities and fertility rates, we calculated each mutant's assembly rate at half-maximal assembly in the absence of profilin and plotted it against its respective fertility rate (Figure 3C). We then drew a

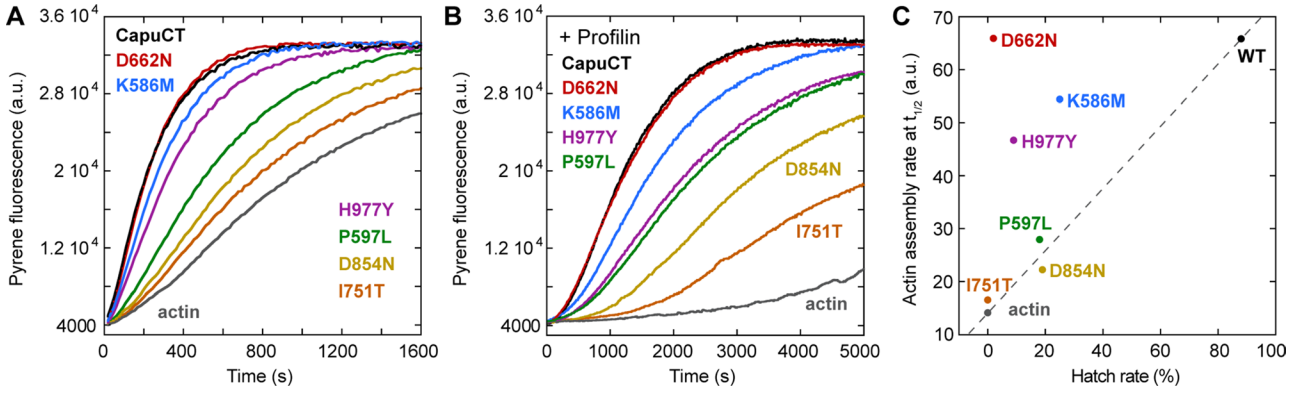

FIGURE 3: Effect of Capu mutations on actin assembly. (A, B) Actin assembly activity of 10 nM of each construct in the absence (A) or presence (B) of 8 μM *S. pombe* profilin (twofold molar excess over actin). (C) Correlation between actin assembly activity (rate at $t_{1/2}$) and fertility (percentage hatched eggs, from Table 1). The dashed line connects wild-type Capu and the actin-alone control to aid in visualization.

hypothetical linear correlation line through wild type and the actin-alone (100% sterile) negative control. Three mutants, CapuCT-P597L, -I751T, and -D854N, fell near the correlation line. The remaining mutants were far removed from this line. Most strikingly, CapuCT-D662N was indistinguishable from wild-type CapuCT in our actin assembly assays despite its deleterious effect in vivo (2% fertility). We conclude that a defect in Capu's actin-assembly activity is not the sole cause of infertility in all cases.

Effect of *capu* mutations on barbed-end elongation and processivity

In addition to promoting actin nucleation, Capu remains processively bound to the actin barbed end, where it can accelerate elongation in the presence of profilin and protect the barbed end from capping protein (Vizcarra *et al.*, 2011; Bor *et al.*, 2012). Elongation activity is difficult to assess in a bulk pyrene-actin assembly assay. To examine each mutation's effect on actin elongation rates and processivity, we monitored the growth of individual actin filaments in the presence of CapuCT using a total internal reflection fluorescence (TIRF) microscope.

Capu accelerates filament elongation about fivefold in the presence of profilin (Bor *et al.*, 2012). Because many profilins, including *Drosophila* profilin (Chic), bind preferentially to unlabeled actin compared with Cys-374 labeled actin, filaments appear dimmer when Capu is bound to the barbed end (Kovar *et al.*, 2006; Bor *et al.*, 2012). Taking advantage of this bias, we measured the barbed-end elongation rate for the Capu-bound dim filaments in the presence of Chic. Analysis of filaments from at least two independent experiments revealed that three mutants, CapuCT-K586M, -P597L, and -H977Y, had significantly lower elongation rates than wild-type CapuCT (Figure 4E). CapuCT-D662N, -I751T, and -D854N had approximately wild-type elongation rates. We then compared the elongation data for these mutants with their respective actin assembly data. Two mutants, CapuCT-P597L and -H977Y, consistently behaved poorly in both assays, and CapuCT-D662N was indistinguishable from wild type in both assays. Of interest, the two weakest mutants in the pyrene-actin assay, CapuCT-I751T and -D854N, had mean elongation rates similar to wild type. In contrast, Capu-K586M had almost wild-type activity in the pyrene-actin assembly assay but had a slower elongation rate, suggesting that nucleation is unaffected by this mutation.

We next examined the processivity of Capu mutants. When 0.6 μM actin was incubated with 1 nM wild-type CapuCT and 3 μM profilin, many fast-growing dim filaments and a few slow-growing bright filaments were present (Figure 4A). CapuCT-D662N showed a similar distribution of dim and bright filaments compared with wild type (Figure 4B). However, with CapuCT-P597L, -I751T, -D854N, and -H977Y, more bright filaments were present than dim filaments (Figure 4, C and D). We also observed many filaments that were initially fast and dim turn into slow, bright filaments, an indication that CapuCT had fallen off of the barbed end. We quantified these events by plotting decay curves. We fit the decay curves with an exponential to obtain an off rate (k_{off}) for each mutant (Figure 4F). Both wild-type CapuCT and CapuCT-D662N had very low off rates, with characteristic run lengths (barbed end growth rate/k_{off}) of ~108,000 subunits (27 subunits s^{-1}/0.00025 s^{-1}) and 81,000 subunits, respectively. CapuCT-K586M, -D854N, and -H977Y had moderate off rates approximately two to five times higher than wild type. CapuCT-P597L and -I751T showed the lowest processivity, with off rates ~10 times higher than wild type and characteristic run lengths of ~9000 subunits.

Our TIRF assay data demonstrate that mutations in the FH2 domain can affect nucleation, elongation, and processivity differentially. Some mutants, such as CapuCT-P597L and -H977Y, had impaired activity in all three areas, suggesting that these residues may be important for the overall integrity of Capu or its ability to bind either actin monomers or filament barbed ends. In contrast, CapuCT-K586M, -I751T, and -D854N exhibited compromised activity in only one or two areas. For example, CapuCT-K586M had nearly wild-type nucleation activity, but its elongation rate and processivity were substantially reduced compared with wild-type. CapuCT-I751T showed the weakest nucleation and processivity, but its elongation activity remained intact. Finally, CapuCT-D854N was compromised in nucleation but had a wild-type elongation rate and near-wild-type processivity. Finally and most strikingly, CapuCT-D662N behaved like wild-type in all three areas.

Effect of mutations on Capu's interactions with known binding partners

Whereas most of our *capu* mutations strongly affected nucleation, elongation, and/or processivity, CapuCT-D662N was indistinguishable from wild type in all of our in vitro actin assembly assays. To understand better how D662N could be causing such a severe phenotype in vivo, we next tested whether D662N or the other mutations affect Capu's interactions with any of its known binding partners.

Two interactions are known to be important for Capu's function in the oocyte: Capu binds the KIND domain of the actin nucleator Spir (Vizcarra *et al.*, 2011; Quinlan, 2013) and is autoinhibited through an intramolecular association between its N-terminal Capu inhibitory domain and C-terminal tail domain (Dahlgaard *et al.*, 2007; Bor *et al.*, 2012). Both Spir-KIND and the N-terminal half of Capu (CapuNT) inhibit CapuCT in bulk pyrene-actin assembly assays (Vizcarra *et al.*, 2011; Bor *et al.*, 2012). Using this assay, we found that Spir-KIND and CapuNT inhibit all of our mutants to approximately the same extent as wild-type CapuCT (Figure 5, A and B). Thus none of our mutations disrupt Capu's interaction with its N-terminal inhibitory domain or the Spir-KIND domain. This is consistent with these interactions being mapped to the Capu-tail as opposed to the FH2 domain (Vizcarra *et al.*, 2011; Bor *et al.*, 2012).

We previously found that mutations in the FH2 domain can alter the interaction between CapuCT and microtubules in vitro (Roth-Johnson *et al.*, 2014). We therefore used high-speed pelleting assays to measure binding of each mutant to Taxol-stabilized microtubules. CapuCT-I751T was omitted from this analysis because it could not be purified at high enough concentrations. Surprisingly, all of the mutants except for CapuCT-D854N bound microtubules at a higher density than wild-type (Figure 5C). These same mutants also bound microtubules with slightly lower affinity than wild type (Table 2). We speculate that this shift in binding density reflects the change in size of the FH2 binding footprint along the microtubule lattice. In other words, a slight change in the conformation of the FH2 domain may have allowed more of these mutants to pack along a given length of the microtubule lattice compared with wild type.

We also tested each mutant's ability to bundle actin filaments in low-speed pelleting assays. Again, CapuCT-I751T was omitted from this analysis due it its low concentration. All mutants except for CapuCT-P597L bundled actin similar to wild type (Figure 5D). CapuCT-P597L showed reduced bundling activity, which was pronounced at higher molar ratios of CapuCT to actin (≥0.1). We note that the F-actin–binding affinity of CapuCT-P597L was not noticeably different from wild type in a high-speed pelleting assay (unpublished data).

With the exception of CapuCT-P597L's compromised F-actin bundling activity, we did not observe any major changes in the

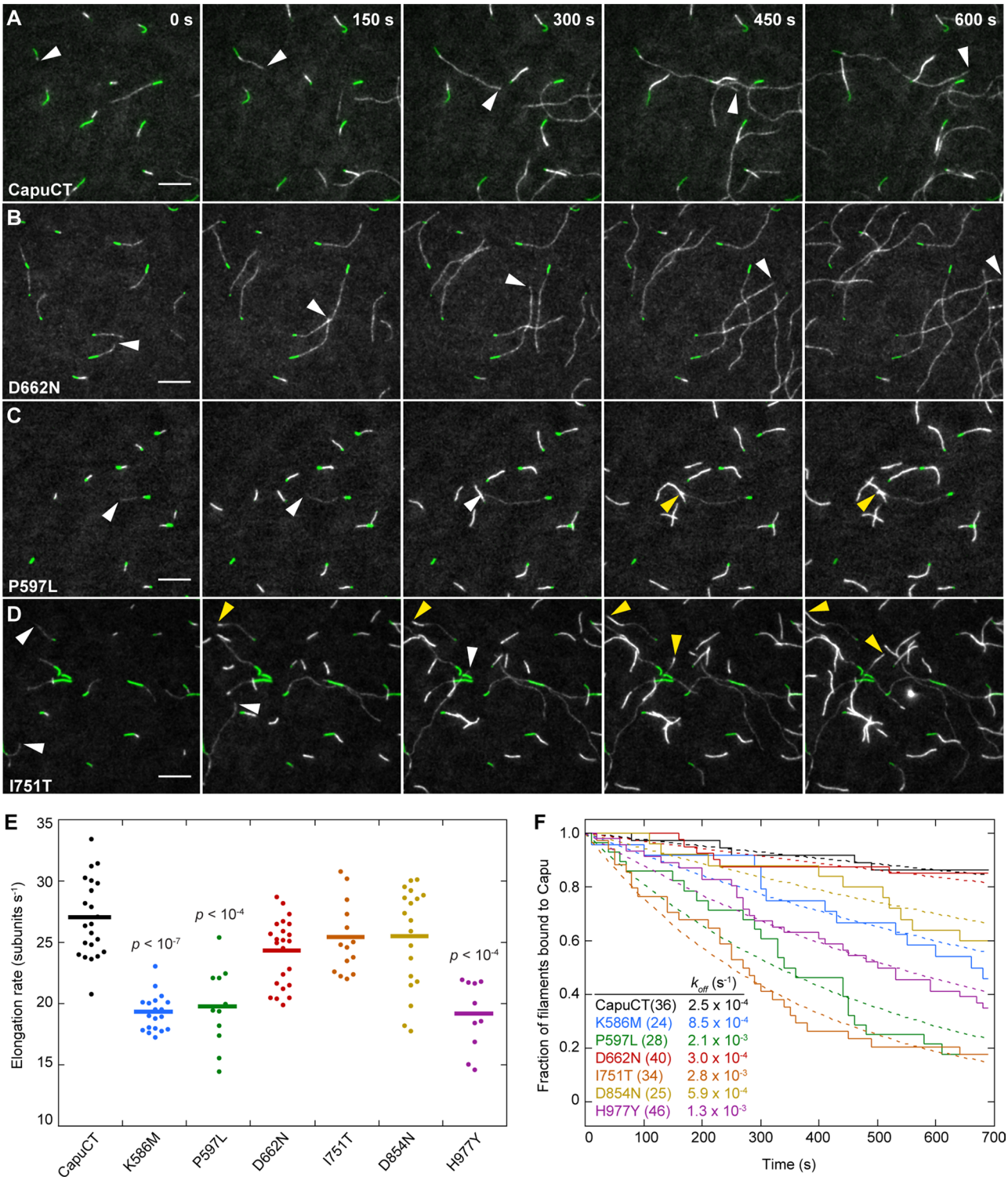

FIGURE 4: Effect of Capu mutations on elongation and processivity. (A–D) TIRF microscopy observation of actin filament (gray) elongation from immobilized F-actin seeds (green) in the presence of wild-type CapuCT or designated mutants. White arrowheads denote the barbed ends of fast-growing dim filaments (CapuCT bound); yellow arrowheads denote the ends of slow-growing bright filaments (no CapuCT bound). Scale bars, 10 μm. The same conditions were used for all TIRF experiments: 0.6 μM actin (20% Oregon green labeled), 1 nM CapuCT, and 3 μM Chic (*Drosophila* profilin). (E) Quantification of elongation rates for CapuCT and CapuCT mutants. At least 10 filaments (represented by dots) were analyzed from at least two independent experiments to obtain the mean elongation rate (represented by a line). The *p* values were calculated using the Mann–Whitney *U* test and are shown for samples that are significantly different from wild-type CapuCT. (F) Quantification of processivity shown as a decay plot. Solid lines represent the fraction of total filaments that have CapuCT bound at the barbed end. The total number of filaments analyzed for each mutant is shown in parentheses. Dashed lines represent the exponential curve fits of the data used to determine k_{off}.

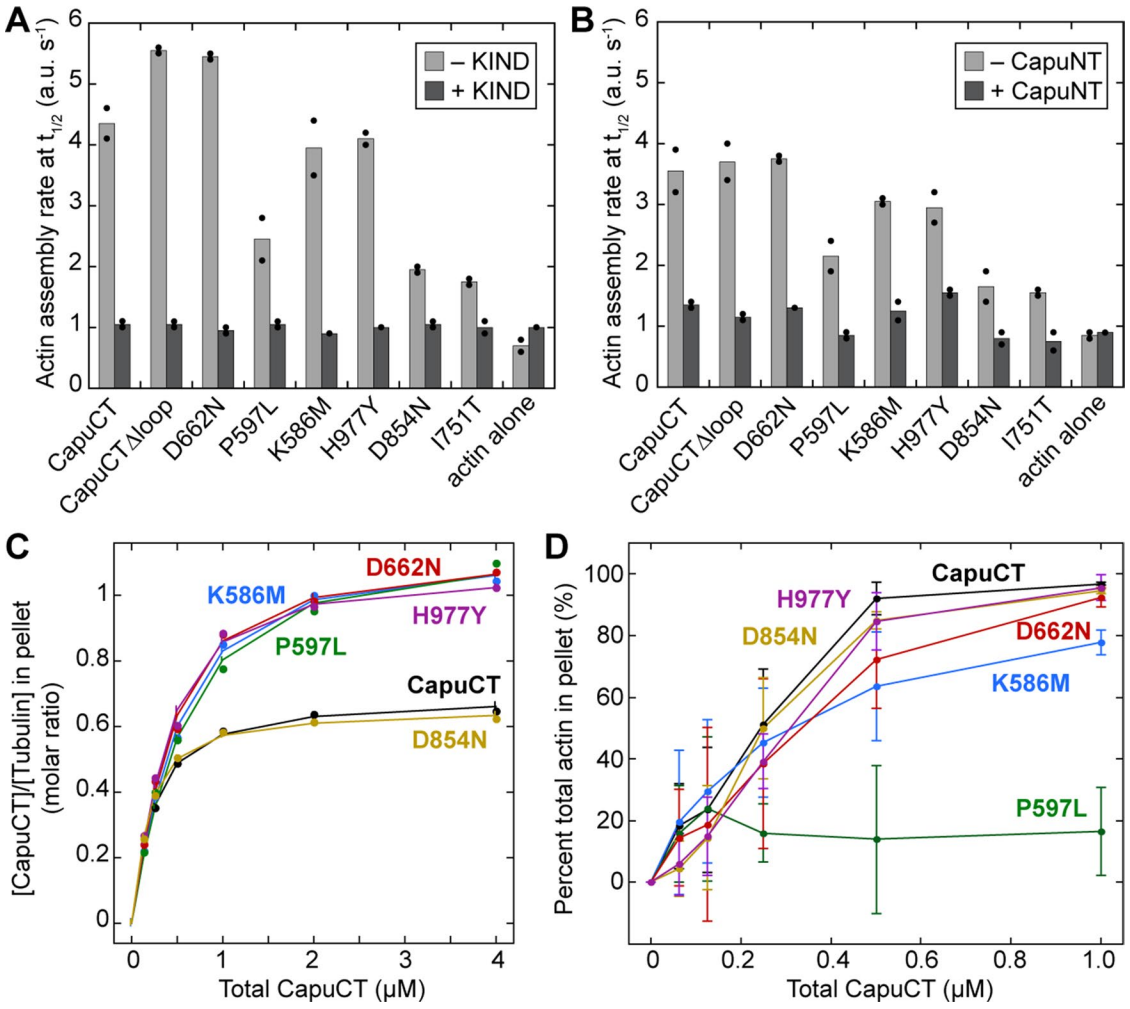

FIGURE 5: Effect of mutations on Capu's interactions with known binding partners. (A, B) Mutations do not affect binding to Spir-KIND or CapuNT. Actin assembly activity (rate at $t_{1/2}$) for each mutant in the absence or presence of either 100-fold molar excess Spir-KIND (A; Spir residues 1–327) or 50-fold molar excess CapuNT (B; Capu residues 1–466). We used 20 nM (wild type, CapuCTΔloop, CapuCT-D662N, -K586M, and -H977Y) or 50 nM (CapuCT-P597L, -D854N, and I751T) CapuCT for each experiment. Bars represent the average of two independent experiments, which are shown as dots. (C) Microtubule binding by each construct compared with wild-type CapuCT at 50 mM KCl with 0.5 μM tubulin. (D) F-actin bundling by each construct compared with wild-type CapuCT at 50 mM KCl with 4 μM actin. Each bundling curve represents the mean of at least four independent experiments, with error bars showing 1 SD.

interactions between the CapuCT mutants and Capu's known binding partners. This is particularly striking for D662N, which behaved similarly to wild type in nearly every in vitro experiment. Although CapuCT-D662N exhibited a slight decrease in microtubule binding affinity and a shift in microtubule binding density, we do not believe that these changes are substantial enough to explain the severe in vivo phenotypes observed for this allele. Although CapuCT-P597L showed reduced F-actin bundling activity, it also has severely compromised actin assembly activity, which correlates well with its effect on fertility (Figure 3C).

Binding experiment	$\Delta_r G$ (kJ/mol)	K_d (μM)	n (α/β dimers per binding site)
CapuCT	4.74 ± 0.11	0.15	1.42 ± 0.01
CapuCT-K586M	3.39 ± 0.14	0.25	0.88 ± 0.01
CapuCT-P597L	2.96 ± 0.22	0.30	0.88 ± 0.02
CapuCT-D662N	3.41 ± 0.17	0.25	0.87 ± 0.01
CapuCT-D854N	5.70 ± 0.13	0.10	1.48 ± 0.01
CapuCT-H977Y	4.27 ± 0.14	0.18	0.95 ± 0.01
CapuCT-ΔLoop	4.39 ± 0.14	0.17	1.30 ± 0.01

Errors for $\Delta_r G$ (the free energy of binding) and n represent 1 SD. The most probable dissociation constant (K_d) values were calculated from $\Delta_r G$ at 25°C. See Roth-Johnson *et al.* (2014) for additional information.

TABLE 2: Fit parameters for all microtubule-binding experiments.

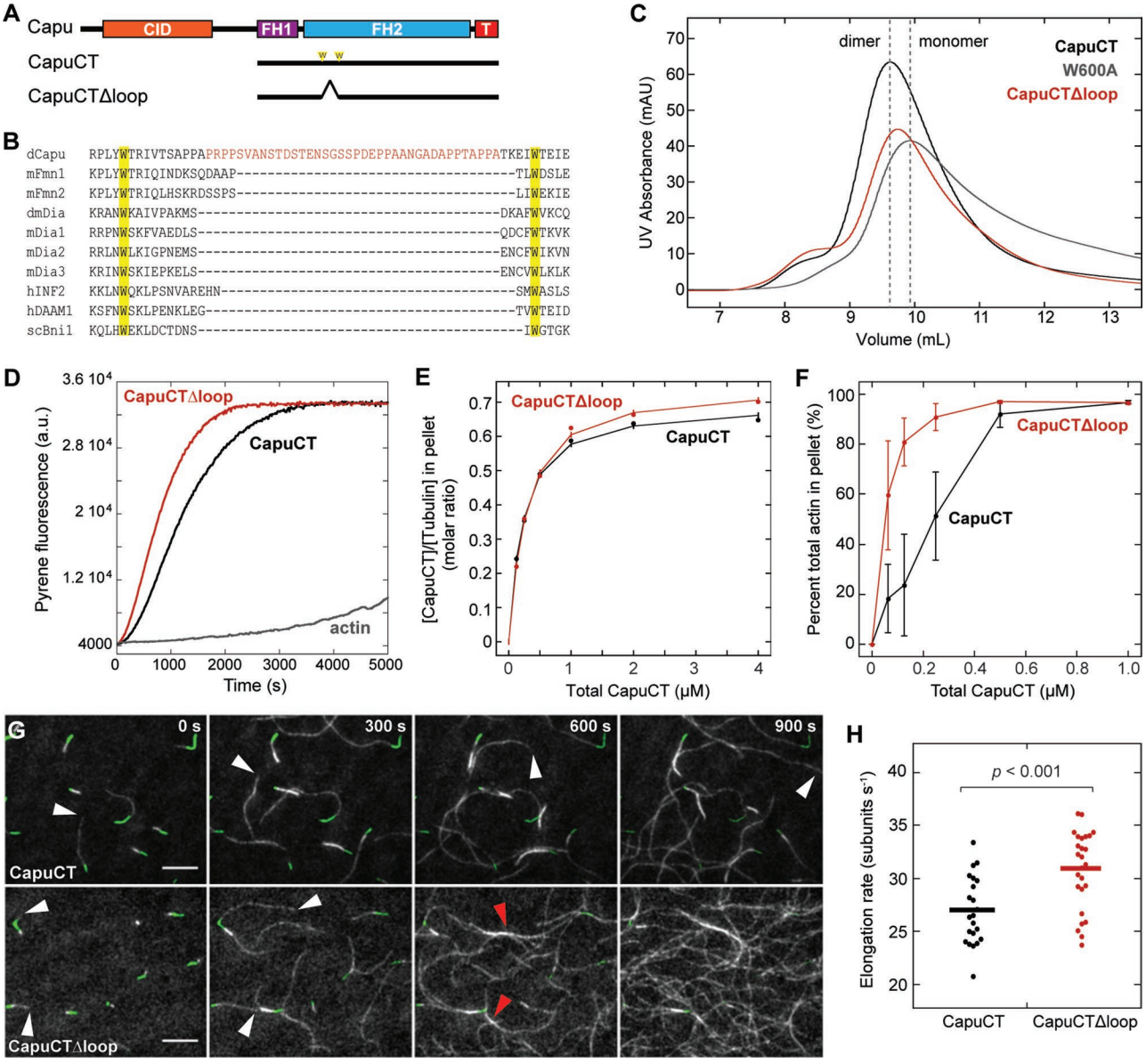

FIGURE 6: Deletion of a "loop" enhances Capu's actin assembly and bundling activity. (A) Domain organization of Capu (1059 amino acids) and schematics of CapuCT and CapuCTΔloop. (B) Sequence alignment showing the location of Capu's extra "loop" domain between the highly conserved lasso Trp residues. (C) Size exclusion chromatography of CapuCTΔloop compared with wild-type CapuCT (dimer) and CapuCT-W600A (monomer) controls. (D) Actin assembly activity of 10 nM CapuCTΔloop in the presence of 8 μM *S. pombe* profilin. (E) Microtubule binding by CapuCTΔloop compared with wild type at 50 mM KCl with 0.5 μM tubulin. (F) F-actin bundling by CapuCTΔloop compared with wild type. Each bundling curve represents the mean of at least four independent experiments, with error bars showing the SD. (G) TIRF microscopy observation of actin filament (gray) elongation from immobilized F-actin seeds (green) in the presence of wild-type CapuCT or CapuCTΔloop. White arrowheads denote the barbed ends of fast-growing dim filaments. Red arrowheads points to F-actin bundles. Scale bar, 10 μm. The same conditions were used for all TIRF experiments: 0.6 μM actin (20% Oregon green labeled), 1 nM CapuCT, and 3 μM Chic (*Drosophila* profilin). (H) Quantification of elongation rates for wild-type CapuCT and CapuCTΔloop. Dots represent individual filaments, and bars represent the mean. The *p* value was calculated using the Mann–Whitney *U* test.

Deletion of a "loop" enhances Capu's nucleation and elongation activity

While studying these *capu* mutations, several of which reside in Capu's lasso region, we noticed that Capu's lasso is substantially longer than those of all other identified formins. Whereas most formins contain 10–20 residues between the two perfectly conserved tryptophan residues in the lasso, Capu contains 52 residues in this region (Figure 6B). We expect this proline-rich lasso insertion to be fairly unstructured and thus refer to it as the "loop" domain.

To begin characterizing this novel loop domain, we created and purified a 38-residue deletion construct (Figure 6A; CapuCTΔloop, residues 467–610 plus 649–1059). In size exclusion chromatography, CapuCTΔloop eluted between the dimer and monomer controls (Figure 6C). This shift could be explained in one of two ways: first, CapuCTΔloop could be in equilibrium between monomer and

dimer; second, removing the loop could make CapuCTΔloop more compact, causing it to elute later than wild-type CapuCT. To distinguish between these two possibilities, we tested the nucleation activity of CapuCTΔloop in bulk pyrene-actin assembly assays. Surprisingly, CapuCTΔloop nucleated actin faster than wild-type CapuCT (Supplemental Figure S3E). The same trend was observed in the presence of profilin and over a range of concentrations (Figure 6D and Supplemental Figure S3F). Because monomeric formins do not nucleate, this supports our second hypothesis, that the deletion of the loop made the protein shape more compact. To probe further the role of this loop region, we examined CapuCTΔloop in all of the assays we used to study the CapuCT point mutants.

Every aspect of CapuCTΔloop actin assembly activity was improved relative to CapuCT. In TIRF microscopy experiments, we found that CapuCTΔloop elongated actin filaments slightly faster than wild-type CapuCT (Figure 6, G and H). With these data, we were able to calculate the concentration of barbed ends produced by wild-type CapuCT and CapuCTΔloop in our bulk polymerization assay (see *Materials and Methods*). With 4 μM actin and 8 μM profilin, the concentration of barbed ends produced by wild-type CapuCT and CapuCTΔloop were 0.08 ± 0.01 and 0.10 ± 0.01 nM, respectively. In agreement with this calculation, we observed that the TIRF field became dense with dim, fast-growing actin filaments more rapidly in the presence of CapuCTΔloop than with wild-type CapuCT. Together our data demonstrate that CapuCTΔloop has higher nucleation and elongation rates than wild-type CapuCT. We could not measure the processivity of CapuCTΔloop because the TIRF field quickly became too crowded for us to confidently track single filaments. However, we believe that CapuCTΔloop has wild-type processivity, if not better, because we did not observe any changes in filament intensity with CapuCTΔloop. We also observed more actin bundles in the presence of CapuCTΔloop. Low-speed pelleting assays showed that CapuCTΔloop indeed bundles F-actin more effectively than wild-type CapuCT (Figure 6F).

We next tested CapuCTΔloop's interaction with other binding partners. Like all of the *capu* mutants, CapuCTΔloop was inhibited by both KIND and CapuNT (Figure 5, A and B). CapuCTΔloop also bound microtubules similarly to wild-type but did exhibit a small increase in microtubule binding density (Figure 6E). On the basis of our size exclusion chromatography experiments, we speculate that removal of the loop region results in a more compact CapuCT dimer, which could have a smaller binding footprint on the microtubule and thus lead to increased binding density. Taking the results together, we conclude that deletion of the "loop" improves overall activity of Capu without disturbing its interaction with other known binding partners in vitro.

DISCUSSION

At the beginning of this study, we had hoped to use EMS-generated *capu* alleles to identify mutations in relatively uncharacterized regions of Capu. We were surprised to find that all of the missense mutations we identified occur in the FH2 domain. We interpret this result as evidence of the physiological importance of the FH2 region. It could also indicate that other regions of Capu are less structurally rigid, making them less susceptible to mutagenesis. Of interest, characterization of the mutations in vitro showed that they have variable effects on Capu's ability to nucleate and elongate actin filaments. Careful analysis of these seven mutations provides new insight into how Capu's FH2 domain assembles actin and which of its activities are important to oogenesis.

Mechanistic insight into FH2 domain function

Mutations in Ile-751 and Leu-768 caused the most severe fertility defects of all the *capu* alleles we tested and were the most poorly behaved in vitro. Based on our homology model, these residues lie next to each other in the hydrophobic core of the knob region of Capu's FH2 domain. We conclude that these two knob mutations disrupt the global structure of Capu, rendering these two alleles effectively nulls.

All of the other mutations appear in the lasso and post regions of Capu's FH2 domain. Of these, D854N (post) is the only mutation on the actin barbed-end–binding surface of the FH2 domain and is located near the conserved residues (Ile-706 and Lys-856) that are important for yeast formin Bni1p association with the actin barbed end (Xu *et al.*, 2004; Quinlan *et al.*, 2007). Thus it is not surprising that CapuCT-D854N had severely compromised actin assembly activity. However, its elongation rate was similar to wild type, and its processivity was only mildly decreased. We therefore speculate that Asp-854 facilitates recruitment of actin monomers to the FH2 domains but is not critical to processive elongation once a filament has formed.

Three of the mutations (K586M, P597L, and H977Y) had reduced elongation rates and compromised processivity. Pro-597 (lasso) and His-977 (post) appear to be similarly semiburied in the FH2 dimer interface, whereas Lys-586 (lasso) appears to be mostly surface exposed. We speculate that the K586M, P597L, and K586M mutations alter the interaction between the two halves of the FH2 dimer, thereby changing the conformation of the FH2 dimer and/or restricting processive movement along the actin barbed end.

Studying these EMS-generated mutations also led us to identify a unique "loop" in the lasso region of Capu's FH2 domain. We showed that deletion of this loop enhances Capu's actin assembly and F-actin bundling activities. We previously found that three mutations in Capu's post region (K851A, K853A, and K858A) similarly enhance Capu's actin assembly activity in bulk assays (Roth-Johnson *et al.*, 2014). Otomo *et al.* (2005) also demonstrated that two knob mutations in Bni1p slightly enhance its in vitro activity. Although rare, mutations that accelerate, rather than slow, a formin's actin assembly activity have now been identified in the loop, post, and knob regions of the FH2 domain. The increased activity of CapuCTΔloop raises an interesting question about the role of the loop: Why would Capu contain a region that makes it a less potent actin nucleator? Perhaps the loop fine-tunes Capu's activity to optimize its physiological function in the oocyte. It is also possible that the loop is important for regulating Capu's activity in vivo through binding interactions and/or posttranslational modifications.

Implications for Capu's role in *Drosophila* oogenesis

During *Drosophila* oogenesis, Capu works together with Spir to build a cytoplasmic actin mesh (Dahlgaard *et al.*, 2007; Quinlan, 2013). We previously showed that Spir and Capu must interact directly to form the actin mesh (Quinlan, 2013). When bound, Spir inhibits Capu's nucleation and elongation activity in vitro (Quinlan *et al.*, 2007; Vizcarra *et al.*, 2011). However, a Capu mutant (I706A) that cannot assemble actin filaments is insufficient to rescue a *capu*-null mutant (Quinlan, 2013). This suggests that Spir and Capu not only interact but must also come apart and function separately to build the actin mesh. Because the I706A mutation disrupts both nucleation and elongation (Vizcarra *et al.*, 2011), it has thus far been impossible to determine which of these activities is required for Capu to build the actin mesh.

In this study, we identified a mutation (D854N) that selectively disrupts nucleation without affecting the elongation rate. Although

	FH2 location	Fertility rate (% hatched)	Stable dimer?	Polymerization rate at $t_{1/2}$ (a.u./s)	Elongation rate (subunits/s)	$k_{off} \times 10^{-5}$ (s^{-1})	Characteristic run length (μm)[a]	Sequence conservation[b]
WT	N/A	88	+	65.8	27.0 ± 3.2	24.5 ± 0.4	300 ± 40	N/A
K586M	Lasso	25	+	54.4	19.3 ± 1.5	85.2 ± 2.3	62 ± 5	++
D854N	Post	19	+	22.2	25.5 ± 4.1	59.2 ± 2.0	120 ± 20	++
P597L	Lasso	18	+	27.9	19.7 ± 3.2	210.0 ± 6.2	26 ± 4	[c]
H977Y	Post	9	+/-	46.7	19.1 ± 2.8	130.0 ± 2.3	40 ± 6	–
D662N	Lasso	2	+	65.9	24.3 ± 2.7	29.7 ± 0.9	220 ± 30	+
L768H	Knob	1	–	n.d.	n.d.	n.d.	n.d.	++
I751T	Knob	0	–	16.6	25.3 ± 2.9	277.0 ± 4.8	25 ± 3	++
Δloop	Lasso	n.d.	+	90.2	30.9 ± 3.7	≥ w.t.	≥ w.t.	–

n.d., not determined.
[a]Characteristic run length = elongation rate (subunits s^{-1})/k_{off} (s^{-1})/365 subunits μm^{-1}.
[b] Degree of sequence conservation was determined by analyzing our sequence alignment (Supplemental Figure S1) with ESPript (http://espript.ibcp.fr; Robert and Gouet, 2014). ++, residues with similarity >70%; +, residues with similarity >30% but <70%; –, no apparent conservation.
[c]Pro-597 is only conserved within the FMN family.

TABLE 3: Summary table.

this mutation decreases Capu's processivity slightly in vitro, its characteristic run length is still >100 μm (the approximate size of a midstage oocyte). Conversely, we found a mutation (K586M) that reduces elongation rate and processivity while only minimally affecting bulk actin assembly activity. Taken together, these findings reveal that both nucleation and elongation are required for Capu to assemble a functional actin mesh in vivo.

We speculated that a long run length is vital in a large cell such as the *Drosophila* oocyte (Vizcarra *et al.*, 2011). Many of the mutations we tested decreased Capu's characteristic run length to well below 100 μm, suggesting that Capu's ability to span the entire length of the oocyte is indeed critical for building the actin mesh. These findings are summarized in Table 3. In this table, we arranged the alleles based on fertility. We observed no correlation with any one of the in vitro actin assembly activities. We interpret this finding to mean that all aspects of actin assembly—nucleation, elongation, and processivity—contribute to building the cytoplasmic actin mesh in vivo.

It was previously proposed that Capu cross-links actin and microtubules in the oocyte (Rosales-Nieves *et al.*, 2006). However, most of the mutations we tested had little effect on Capu's ability to bind microtubules or bundle F-actin. Most mutations caused a shift in microtubule binding density very similar to the shift observed for several other FH2 mutations (Roth-Johnson *et al.*, 2014). However, every mutant still bound microtubules with submicromolar affinity, suggesting that the shift in binding density is not directly responsible for the phenotypes observed during oogenesis. It is also unclear whether the CapuCT-P597L's reduced F-actin–bundling activity is physiologically relevant. If anything, the fact that removing Capu's "loop" increases CapuCT's F-actin–bundling activity suggests that too much F-actin bundling may be detrimental to the oocyte. A constitutively active Capu construct causes an overabundance of actin that is deleterious in vivo (Bor *et al.*, 2015). Similarly, high degrees of bundling might lead to an overly dense and/or stable mesh.

Intriguingly, CapuCT-D662N was nearly indistinguishable from wild type in every in vitro assay we performed. Although D662N may cause a slight reduction in elongation rate and processivity, its characteristic run length (220 μm) is still much larger than a typical midstage oocyte. We hypothesize that D662N disrupts an unknown binding interaction and/or regulatory aspect of Capu's function in the oocyte. The study that first described the D662N mutation showed that Capu forms a tertiary complex with Spir and the Golgi/endosomal protein Mon2 (Tanaka *et al.*, 2011). D662N could disrupt the formation of this complex, leading to the developmental defects we observed. Alternatively, several formins are regulated through posttranslational modifications, which can alter autoinhibition and binding to microtubules (Takeya *et al.*, 2008; Cheng *et al.*, 2011; Staus *et al.*, 2011). Perhaps D662N lies near a phosphorylation site or is required for binding to a kinase or other regulatory protein. Improper regulation of Capu in vivo could explain the severe mesh and fertility defects we observed.

Concluding remarks

Analysis of seven EMS-generated *capu* mutants highlights the functional importance of the FH2 domain. We identified mutations that selectively disrupt either nucleation (D854N) or elongation (K586M), both of which are highly conserved residues, providing important mechanistic insight into formin function and Capu's role in the *Drosophila* oocyte, as well as potential tools to study other formins. We also identified a mutation (D662N) that showed no notable defects in vitro despite exhibiting severe defects in vivo. Further examination of this mutation will likely provide important information about Capu's regulation during oogenesis. Finally, our data suggest that the lasso and post regions are likely hot spots for identifying new mutations that not only impair but also enhance formin activity. Such mutations that selectively disrupt or enhance formin processivity, elongation rate, and nucleation will be valuable tools for studying how all formins function in vitro and in vivo.

MATERIALS AND METHODS

Drosophila stocks

The wild-type stock (w^{1118}) and the deficiency stock (Df(2L)ed-dp/SM1) were obtained from the Bloomington Stock Center (Bloomington, IN). $capu^{A354}$ flies were provided by Akira Nakamura (RIKEN, Kobe, Japan; Tanaka *et al.*, 2011). $capu^{L201}$, and $capu^{L219}$ flies were provided by Stefan Luschnig (University of Zurich, Zurich, Switzerland) and the Tübingen *Drosophila* Stock Collection (Tübingen, Germany; Luschnig, 2004). $capu^{1}$, $capu^{HK}$, $capu^{38}$, and $capu^{2F}$ flies

were provided by Trudi Schupbach (Princeton University, Princeton, NJ; Manseau and Schupbach, 1989; Emmons *et al.*, 1995).

Fertility assays

Fertility assays were performed as described previously (Quinlan, 2013). Each trial was repeated three times with independent crosses.

Microscopy and streaming analysis

For all experiments, flies were fattened with yeast paste overnight before imaging. Visualization of cytoplasmic streaming and the actin mesh were performed on a Leica SPE I inverted confocal microscope.

The actin mesh was stained as previously described, but with slight modifications (Dahlgaard *et al.*, 2007). Briefly, ovaries were dissected, teased apart, and fixed in 10% paraformaldehyde/phosphate-buffered saline (PBS). Samples were stained with 1 µM Alexa Fluor 647–phalloidin (Life Technologies, Carlsbad, CA), washed extensively with PBS, and mounted in ProLong Gold (Life Technologies). Images were recorded within 24 h of staining because phalloidin disassociates from actin over time (Dahlgaard *et al.*, 2007).

Cytoplasmic movements were examined in living oocytes with $\lambda_{excitation}$ = 405 nm to visualize autofluorescence of yolk granules. Time-lapse movies of oocytes were recorded by acquiring 1 frame every 10 s for 3–5 min. Standard deviation *z*-projections were created in Fiji to demonstrate the relative motion of yolk granules. Cytoplasmic streaming velocities were determined from confocal movies using custom-built particle image velocimetry as previously described (Quinlan, 2013).

Identification and confirmation of *capu* lesions

To identify *capu* mutations, ovaries were dissected from homozygous female flies fattened with yeast paste in cold, ionically matched adult *Drosophila* saline buffer (Singleton and Woodruff, 1994). RNA was isolated from the ovaries using the RNeasy Mini Kit (Qiagen, Valencia, CA) according to the manufacturer's instructions for animal tissue samples. cDNA was generated using the Maxima Universal First Strand cDNA Synthesis Kit (Fermentas/Thermo Scientific, Waltham, MA), subcloned into the pJET1.2 vector (Fermentas), and sequenced (GENEWIZ, La Jolla, CA).

To confirm previously reported and newly identified lesions, genomic DNA was isolated from single flies as previously described (Gloor and Engels, 1992). The DNA region around each reported mutation site was PCR amplified using intronic primers. Amplified PCR products from at least two flies from each fly line were sequenced (GENEWIZ).

DNA constructs and cloning

Wild-type CapuCT (amino acids 467–1059) and mutant constructs were subcloned into a modified version of pET-15b with an N-terminal hexahistidine tag as previously described (Vizcarra *et al.*, 2011). Point mutations were created using QuikChange mutagenesis (Stratagene, La Jolla, CA). CapuCTΔloop (amino acids 467–610 plus 649–1059) was created using the gene splicing by overlap extension method of PCR (Horton *et al.*, 1990).

Protein expression and purification

Acanthamoeba castellani actin, Chickadee (*Drosophila* profilin), and *S. pombe* profilin were purified following published protocols (MacLean-Fletcher and Pollard, 1980; Bor *et al.*, 2012). CapuNT (Bor *et al.*, 2012) and CapuCT constructs (Vizcarra *et al.*, 2011) were purified as previously described. Briefly, CapuCT proteins were expressed in Terrific Broth medium at 37°C to an OD_{600} of 0.7, induced with 0.25 mM isopropyl-β-D-thiogalactoside at 18°C, and harvested 18 h later. Then the protein was purified with Talon resin (Clontech, Mountain View, CA) and MonoQ anion exchange chromatography (GE Healthcare). The concentrations of the mutant constructs were calculated based on quantitative Sypro-Red (Invitrogen) staining with wild-type CapuCT as a standard.

Size exclusion chromatography

A Superdex 200 size exclusion column (GE Healthcare) was equilibrated with column buffer (50 mM 4-(2-hydroxyethyl)-1-piperazineethanesulfonic acid [HEPES], pH 7, 150 mM NaCl, 1 mM dithiothreitol [DTT]). Approximately 4 nmol of each CapuCT construct was diluted in column buffer, centrifuged at 100,000 × *g* for 20 min at 4°C, and loaded onto the equilibrated column. Wild-type CapuCT and CapuCT-W600A were used as dimer and monomer controls, respectively. For CapuCT-H977Y, a peak dimer fraction was taken, centrifuged at 100,000 × *g* for 20 min at 4°C, and loaded on the column a second time.

Pyrene-actin polymerization assay

Pyrene-actin polymerization assays were performed essentially as described (Zalevsky *et al.*, 2001) with minor modifications (Bor *et al.*, 2012). Briefly, 4 µM 5% pyrene-labeled actin was incubated for 2 min in ME buffer (200 µM ethylene glycol tetraacetic acid [EGTA] and 50 µM $MgCl_2$) to convert Ca-actin to Mg-actin. Polymerization was initiated by adding KMEH buffer (final concentration: 10 mM Na-HEPES, 1 mM EGTA, 50 mM KCl, and 1 mM $MgCl_2$) to the Mg-actin. Additional components, such as CapuCT, CapuNT, and KIND, were added to the KMEH buffer before addition to Mg-actin. For experiments in the presence of profilin, *S. pombe* profilin was briefly preincubated with the Mg-actin before addition of KMEH and other assay components. Pyrene fluorescence was measured by a TECAN F200 (TECAN US, Morrisville, NC) with $\lambda_{excitation}$ = 365 nm and $\lambda_{emission}$ = 407 nm. Barbed-end concentrations were calculated by dividing the slope at $t_{1/2}$ by the elongation rate measured in TIRF experiments. The unit for the slope was converted from arbitrary units/second to micromoles/second by normalizing the minimum and the maximum arbitrary units to 0 and 3.9 µM actin, respectively.

TIRF microscopy

Coverslips were silanized and functionalized with biotin–polyethylene glycol as described (Hansen and Mullins, 2010; Bor *et al.*, 2012). We prepared 15-µl flow cells for imaging as previously described (Vizcarra *et al.*, 2014). The final conditions in the flow chambers were as follows: 0.6 µM Mg-G-actin (13.5–20% Oregon green labeled) in 1× KMEH, 3 µM profilin (Chic), 1 nM CapuCT, 0.2% methylcellulose, 50 mM DTT, 0.2 mM glucose, 250 µg/ml glucose oxidase, and 50 µg/ml catalase. Growing actin filaments were visualized on a DMI6000 TIRF microscope (Leica, Germany) by acquiring images every 10 s for 10 min. Filament elongation rates were analyzed with the JFilament plug-in in FIJI (Smith *et al.*, 2010; Schindelin *et al.*, 2012). Processivity was analyzed by counting the total number of Capu-associated filaments in the initial frame and calculating the ratio of currently Capu-associated filaments to the initial total number of Capu-associated filaments at each frame over a period of ~12 min (~70 frames).

Microtubule and actin cosedimentation assays

Tubulin was purchased from Cytoskeleton (T240, lot 85; Denver, CO). Microtubule preparation, binding experiments, and analysis were all performed as described (Roth-Johnson *et al.*, 2014). Actin bundling assays were performed as described (Vizcarra *et al.*, 2014).

ACKNOWLEDGMENTS

We thank Justin Bois for help with particle image velocimetry, Andrey Shur for training an undergraduate in actin purification, Christina L. Vizcarra for help with TIRF microscopy, and other members of the Quinlan and Reisler labs for useful discussions. H.Y. especially thanks M. E. Quinlan for generously offering her a position in the Quinlan lab and E. A. Roth-Johnson for guiding her in the right direction whenever she ran into a problem and nurturing her to become a productive member of the lab. This work was supported by National Institutes of Health Ruth L. Kirschstein National Research Service Award GM007185 (to E.A.R.-J.), National Institutes of Health National Institute of General Medical Sciences Grant R01 GM096133, a Burroughs Wellcome Fund Career Award in the Biomedical Sciences, and March of Dimes Foundation Grant 1-FY12-442 (to M.E.Q.). Stocks obtained from the Bloomington *Drosophila* Stock Center (National Institutes of Health Grant P4OD018537) were used in this study.

REFERENCES

Arnold K, Bordoli L, Kopp J, Schwede T (2006). The SWISS-MODEL workspace: a web-based environment for protein structure homology modelling. Bioinformatics 22, 195–201.

Bor B, Bois JS, Quinlan ME (2015). Regulation of the formin Cappuccino is critical for polarity of Drosophila oocytes. Cytoskeleton 72, 1–15.

Bor B, Vizcarra CL, Phillips ML, Quinlan ME (2012). Autoinhibition of the formin Cappuccino in the absence of canonical autoinhibitory domains. Mol Biol Cell 23, 3801–3813.

Cheng L, Zhang J, Ahmad S, Rozier L, Yu H, Deng H, Mao Y (2011). Aurora B regulates formin mDia3 in achieving metaphase chromosome alignment. Dev Cell 20, 342–352.

Dahlgaard K, Raposo AASF, Niccoli T, St Johnston D (2007). Capu and spire assemble a cytoplasmic actin mesh that maintains microtubule organization in the Drosophila oocyte. Dev Cell 13, 539–553.

Emmons S, Phan H, Calley J, Chen W, James B, Manseau L (1995). Cappuccino, a Drosophila maternal effect gene required for polarity of the egg and embryo, is related to the vertebrate limb deformity locus. Genes Dev 9, 2482–2494.

Gloor GB, Engels WR (1992). Single-fly DNA preps for PCR. Drosoph Inf Serv 71, 148–149.

Hansen SD, Mullins RD (2010). VASP is a processive actin polymerase that requires monomeric actin for barbed end association. J Cell Biol 191, 571–584.

Horton RM, Cai ZL, Ho SN, Pease LR (1990). Gene splicing by overlap extension: tailor-made genes using the polymerase chain reaction. BioTechniques 8, 528–535.

Kovar DR, Harris ES, Mahaffy R, Higgs HN, Pollard TD (2006). Control of the assembly of ATP- and ADP-actin by formins and profilin. Cell 124, 423–435.

Lu J, Meng W, Poy F, Maiti S, Goode BL, Eck MJ (2007). Structure of the FH2 domain of Daam1: implications for formin regulation of actin assembly. J Mol Biol 369, 1258–1269.

Luschnig S, Moussian B, Krauss J, Desjeux I, Perkovic J, Nüsslein-Volhard C (2004). An F1 genetic screen for maternal-effect mutations affecting embryonic pattern formation in Drosophila melanogaster. Genetics 167, 325–342.

MacLean-Fletcher S, Pollard TD (1980). Identification of a factor in conventional muscle actin preparations which inhibits actin filament self-association. Biochem Biophys Res Commun 96, 18–27.

Manseau LJ, Schupbach T (1989). cappuccino and spire: two unique maternal-effect loci required for both the anteroposterior and dorsoventral patterns of the Drosophila embryo. Genes Dev 3, 1437–1452.

Otomo T, Tomchick DR, Otomo C, Panchal SC, Machius M, Rosen MK (2005). Structural basis of actin filament nucleation and processive capping by a formin homology 2 domain. Nature 433, 488–494.

Pruyne D (2002). Role of formins in actin assembly: nucleation and barbed-end association. Science 297, 612–615.

Quinlan ME (2013). Direct interaction between two actin nucleators is required in Drosophila oogenesis. Development 140, 4417–4425.

Quinlan ME, Heuser JE, Kerkhoff E, Dyche Mullins R (2005). Drosophila Spire is an actin nucleation factor. Nature 433, 382–388.

Quinlan ME, Hilgert S, Bedrossian A, Mullins RD, Kerkhoff E (2007). Regulatory interactions between two actin nucleators, Spire and Cappuccino. J Cell Biol 179, 117–128.

Robert X, Gouet P (2014). Deciphering key features in protein structures with the new ENDscript server. Nucleic Acids Res 42, (W1), W320–W324.

Rosales-Nieves AE, Johndrow JE, Keller LC, Magie CR, Pinto-Santini DM, Parkhurst SM (2006). Coordination of microtubule and microfilament dynamics by Drosophila Rho1, Spire and Cappuccino. Nat Cell Biol 8, 367–376.

Roth-Johnson EA, Vizcarra CL, Bois JS, Quinlan ME (2014). Interaction between microtubules and the Drosophila formin cappuccino and its effect on actin assembly. J Biol Chem 289, 4395–4404.

Schindelin J, Arganda-Carreras I, Frise E, Kaynig V, Longair M, Pietzsch T, Preibisch S, Rueden C, Saalfeld S, Schmid B, *et al.* (2012). Fiji: an open-source platform for biological-image analysis. Nat Methods 9, 676–682.

Singleton K, Woodruff RI (1994). The osmolarity of adult Drosophila hemolymph and its effect on oocyte-nurse cell electrical polarity. Dev Biol 161, 154–167.

Smith MB, Li H, Shen T, Huang X, Yusuf E, Vavylonis D (2010). Segmentation and tracking of cytoskeletal filaments using open active contours. Cytoskeleton 67, 693–705.

Staus DP, Taylor JM, Mack CP (2011). Enhancement of mDia2 activity by Rho-kinase-dependent phosphorylation of the diaphanous autoregulatory domain. Biochem J 439, 57–65.

Takeya R, Taniguchi K, Narumiya S, Sumimoto H (2008). The mammalian formin FHOD1 is activated through phosphorylation by ROCK and mediates thrombin-induced stress fibre formation in endothelial cells. EMBO J 27, 618–628.

Tanaka T, Kato Y, Matsuda K, Hanyu-Nakamura K, Nakamura A (2011). Drosophila Mon2 couples Oskar-induced endocytosis with actin remodeling for cortical anchorage of the germ plasm. Development 138, 2523–2532.

Theurkauf WE (1994). Premature microtubule-dependent cytoplasmic streaming in cappuccino and spire mutant oocytes. Science 265, 2093–2096.

Vizcarra CL, Bor B, Quinlan ME (2014). The role of formin tails in actin nucleation, processive elongation, and filament bundling. J Biol Chem 289, 30602–30613 .

Vizcarra CL, Kreutz B, Rodal AA, Toms AV, Lu J, Zheng W, Quinlan ME, Eck MJ (2011). Structure and function of the interacting domains of Spire and Fmn-family formins. Proc Natl Acad Sci USA 108, 11884–11889.

Xu Y, Moseley JB, Sagot I, Poy F, Pellman D, Goode BL, Eck MJ (2004). Crystal structures of a formin homology-2 domain reveal a tethered dimer architecture. Cell 116, 711–723.

Zalevsky J, Grigorova I, Mullins RD (2001). Activation of the Arp2/3 complex by the Listeria acta protein. Acta binds two actin monomers and three subunits of the Arp2/3 complex. J Biol Chem 276, 3468–3475.